

Contents lists available at ScienceDirect

Carbon

journal homepage: www.elsevier.com/locate/carbon



Research Article

Pore size characterization of micro-mesoporous carbons using CO₂ adsorption[★]



Silvio Dantas ^a, Katie Cychosz Struckhoff ^b, Matthias Thommes ^{c, **}, Alexander V. Neimark ^{a, *}

- a Department of Chemical and Biochemical Engineering, Rutgers, The State University of New Jersey, 98 Brett Road, Piscataway, NJ, 08854, United States
- ^b Anton Paar Quantatec Inc., 1900 Corporate Dr, Boynton Beach, FL, 33426, United States
- ^c Department of Chemical and Bioengineering, Institute of Separation Science and Technology, Friedrich-Alexander University Erlangen-Nürnberg, 91058, Erlangen, Germany

ARTICLE INFO

Article history: Received 24 September 2020 Received in revised form 19 November 2020 Accepted 20 November 2020 Available online 25 November 2020

Keywords:
Gas adsorption
Pore size characterization
Nanoporous materials
Carbons
Carbon dioxide adsorption

ABSTRACT

Pore structure characterization plays a crucial role in the optimization of adsorption properties of nanoporous carbons employed for water purification, gas and liquid phase separations, carbon dioxide reduction, energy storage, and other applications. Here, we present an original methodology for evaluating the pore size distribution in carbons in a wide range of micro- and mesopores from 0.385 to 10 nm from a single isotherm of high-pressure adsorption of CO₂ at 273 K. The proposed method is based on the reference theoretical isotherms calculated by Monte Carlo simulations in model pores of slit-shaped and cylindrical geometry. The relationship between the pore size and the pore filling pressure is established. Special attention is given to the predicting of the capillary condensation transitions in mesopores by using the meso-canonical ensemble (gauge cell) Monte Carlo simulations. The proposed technique is demonstrated and verified against the conventional N₂ and Ar low temperature adsorption methods drawing on the example of micro-mesoporous carbons of the CMK family. Advantages and limitations of CO₂ adsorption characterization of nanoporous materials are discussed and further improvements are proposed.

© 2020 Elsevier Ltd. All rights reserved.

1. Introduction

The problems of pore size characterization of nanoporous carbons have been attracting continuous attention in the materials science and adsorption communities, starting from the ground-breaking works of Professor Francisco (Paco) Rodriguez-Reinoso, which expanded our understanding of the relationships between the structural and engineering properties of carbon materials and their applications [1–5]. Over the past several decades, nanoporous carbon materials have been extensively used in both industrial and consumer applications. With their high microporosity, carbon-based materials are well suited for many purposes including capture and sequestration of gases [6], filtration processes [7], energy storage [8], catalysis [9]. As the search for new materials continued,

E-mail addresses: matthias.thommes@fau.de (M. Thommes), aneimark@rutgers.edu (A.V. Neimark).

advanced templating procedures were developed and brought about the synthesis of ordered mesoporous carbon materials [10–15]. The ability to tune the pore structure enables the synthesis of materials with large pore surface area and pore volume. With that ability comes the need to properly understand the textural properties (e.g., surface area, pore size) of these materials to improve their use in catalysis, separations, and many other applications [16]. While N_2 and Ar gas adsorption at cryogenic temperatures are often used to characterize carbon materials, CO_2 has been shown to be an effective probe molecule due to faster diffusion rates and better penetration into micropores at ambient temperatures [1,17]. As such, it is desirable to have characterization techniques based on gas adsorption using CO_2 as a molecular probe to directly determine the distribution of pores accessible to CO_2 and their maximum capacity in the wide range of pressures.

Until recently, CO₂ adsorption was used exclusively for accessing micropores, mostly due to pressure limitations (below 1 atm) on the instrumentation for CO₂ adsorption measurements [18]. Within this limited pressure range, CO₂ does not fill the micropores larger than ~1 nm, consequently restricting the reliable pore size analysis to ultramicropores smaller 0.8 nm. Recent improvements in adsorption

^{*} Dedicated to the legacy of Francisco (Paco) Rodriguez-Reinoso, the pioneer in nanoporous carbon synthesis and characterization.

^{*} Corresponding author.

^{**} Corresponding author.

instrumentation technology enabled the access of a wide range of relative pressures, from ultra-high vacuum ($p/p_0 = 10^{-7}$) to high pressures (<75 bar), meaning that CO₂ adsorption isotherms can be measured at 0 °C up to the saturation, $p/p_0 = 1$ or 34.85 bar [19]. The increase of the pressure range makes it possible to obtain the pore size distributions (PSDs) over a wide micro- and mesopore range from a single CO₂ adsorption experiment. Noteworthy, the use of CO₂ for pore size analysis is only recommended for non-polar materials such as carbons without an appreciable amount of polar surface functionality, as its large quadrupole moment makes it difficult to correlate the pore filling pressure with pore size [5]. The conversion of the adsorption isotherm into the pore size distribution requires a theoretical model for calculating the kernel of reference adsorption isotherms in pores of different sizes. Here, we employ Monte Carlo (MC) simulations to produce in-silico generated kernels of adsorption and desorption isotherms of CO₂ at 273 K up to the saturation pressure (34.85 bar), covering a wide range of micro- and mesopores (0.385-10 nm).

Several methods are available for porous materials characterization from adsorption isotherms [18]. The density functional theory (DFT) methods [20] are particularly useful for their ability to provide pore size, surface area, and volume distributions for the entire micromesopore range. In earlier works [21,22], it was shown that non-local density functional theory (NLDFT) with a specially parameterized Lennard-Jones model of CO₂ molecule produces similar adsorption isotherms as Grand Canonical Monte Carlo (GCMC) simulations in the micropore range. GCMC has been implemented to obtain PSDs using slit and mixed geometries and Lennard-Iones models for N₂ and CO₂ applied to activated carbons [23], and more recently, N₂ applied to CMK-3 carbons [24]. DFT adsorption kernels were developed and applied for PSD characterization of micro-mesoporous carbons from N₂ and Ar isotherms [22,25,26]. However, the DFT methods, which are based on a simplistic Lennard-Jones model of the CO2 molecule, cannot capture the specifics of CO₂ adsorption in mesopores at high pressures, especially in the region of adsorption hysteresis that is observed in the simulations at 273 K in pores larger 5.5 nm. The advanced methods of MC simulations using multicenter models of the CO₂ molecule are required. In this work, we employ GCMC and gauge cell meso-canonical MC (MCMC) [27-29] simulations to generate the kernels of theoretical adsorption and desorption isotherms for slit and cylindrical carbon pores with sizes ranging from micropores to mesopores. Based on these kernels, we suggest a novel PSD calculation method. The method is demonstrated on well characterized samples of CMK-3 micro-mesoporous carbons, which possess a multiscale structure of ordered mesopore channels within a microporous skeleton. Despite the mesopore channels in CMK-3 carbons having a complex shape, the cylindrical pore approximation provides the characteristic pore diameters in compliance with the results of independent XRD studies [30].

2. Methodology

2.1. Pore size distribution (PSD) calculations

The PSD, $\phi(D)$, is calculated by comparing the experimental isotherm, $N^{exp}(P/P_0)$, and a set (kernel) of reference isotherms, $N^{sim}(D, P/P_0)$, produced in MC simulations in a series of model

pores within a range of pore diameters, D, from D_{\min} to D_{\max} . The experimental isotherm, $N^{exp}(P/P_0)$, is interpreted as a superposition of the reference isotherms $N^{sim}(D, P/P_0)$, weighted with the PSD, $\phi(D)$, according to the integral adsorption equation, eq. (1).

$$N^{exp}(P/P_0) = \int_{D_{col}}^{D_{max}} \phi(D) N^{sim}(D, P/P_0) dD$$
 (1)

To find a solution for the PSD, eq. (1) is represented as a matrix equation, solved using the quick non-negative least square method (QNNLS) [31]. The QNNLS is based on an adaptable procedure that combines Tikhonov regularization method [32] with the non-negative least squares algorithm [33].

2.2. Experimental isotherms

The micro-mesoporous carbon samples [34,35] were outgassed at 423 K for 12 h under turbomolecular pump vacuum. Ar (87 K) and N_2 (77 K) adsorption measurements were performed on Autosorb-iQ MP, and CO_2 (273 K) measurements on iSorb HP from Quantachrome Instruments. CMK-3 was synthesized according to the methods given by Ryoo [36] and Huwe [34]. Hereafter, the samples are referred to as CMK-3a, CMK-3b and CMK-3c.

2.3. Theoretical isotherms

The model carbon pore structure is presented as composed of perfectly smooth, non-flexible, and infinitely long cylindrical [37] or slit-shaped [38] pores. The CO₂ molecule is modeled using the TraPPE model [39] with the 15 Å cutoff. Solid-fluid potential is applied to a cubic cell with periodic boundary conditions on all three axes with "padding" of half of the cutoff distance added to the outside of the pore. The Lennard Jones (LJ) parameters of interactions between O and C atoms employed in the simulations are as follows [40]: $\sigma_{\rm O-O}=0.305\,nm$, $\varepsilon_{\rm O-O}/k_b=79\,K$, $\sigma_{\rm s-O}=0.3225\,nm$, $\varepsilon_{\rm s-O}/k_b=46.184\,K$, $\sigma_{\rm C-C}=0.28\,nm$, $\varepsilon_{\rm C-C}/k_b=27\,K$, $\sigma_{\rm s-C}=0.31\,nm$, and $\varepsilon_{\rm s-C}/k_b=27\,K$, where k_b is the Boltzmann constant. The solid-fluid interaction parameters are calculated using Lorentz-Berthelot mixing rules with the fluidfluid parameters from TraPPE, and solid-solid parameters determined from fitting of the experimental data [41], $\sigma_{s-s} = 0.34 \, nm$ and $\varepsilon_{s-s}/k_b=27\,K$. The simulations are performed using the MCCCS Towhee software package [42] with the addition of the LI potential from a cylindrical surface (eq. (3)), which was implemented as part of an earlier work [40]. Equations for the solidfluid potentials are shown below, where z and r are, respectively, the center-to-center distances between the fluid atom (O or C) and the pore wall of slit (eq. (2)) pores, and the center of the cylindrical (eq. (3)) pores. Pore width is defined as $D_{in} =$ $D_{center-to-center} - \sigma_{s-s}$. Finally, ρ_A is the area density of carbon atoms in the pore surface, $\rho_A = 38.19 \, nm^{-2}$.

$$U_{sf}(z) = 2\pi \rho_A \sigma_{sf}^2 \varepsilon_{sf} \left[\frac{2}{5} \left(\frac{\sigma_{sf}}{z} \right)^{10} - \left(\frac{\sigma_{sf}}{z} \right)^4 - \frac{\sigma_{sf}^4}{3\Delta (z + \alpha \Delta)^3} \right]$$
(2)

$$U_{sf}(r) = \pi^{2} \rho_{A} \sigma_{sf}^{2} \varepsilon_{sf} \left[\frac{63}{32} F\left(-\frac{9}{2}, -\frac{9}{2}, 1, \left(\frac{r}{R} \right)^{2} \right) \left(\frac{\sigma_{sf} R}{\left(R^{2} - r^{2} \right)} \right)^{10} - 3F\left(-\frac{3}{2}, -\frac{3}{2}, 1, \left(\frac{r}{R} \right)^{2} \right) \left(\frac{\sigma_{sf} R}{\left(R^{2} - r^{2} \right)} \right)^{4} \right]$$

$$(3)$$

GCMC method is used to calculate the density of the adsorbate under the confinement of the pore walls. The simulation box has dimensions of 3.05 nm \times 3.05 nm \times ($D_{in} + \sigma_{s-s} + 1.5$) nm for slit pores and 3.05 nm \times ($D_{in} + \sigma_{s-s} + 1.5$) nm \times ($D_{in} + \sigma_{s-s} + 1.5$) nm for cylindrical pores. Each isotherm is calculated using at least 100 values of the adsorbate chemical potential corresponding to the relative pressures, p/p_0 , distributed with the range from 10^{-9} to 1. Results are averaged over a minimum of 2×10^6 steps after being equilibrated for at least 4×10^5 steps.

In the mesopores, where the GCMC isotherms exhibit capillary condensation hysteresis loop formed by metastable adsorption and desorption branches, the gauge cell meso-canonical MC (MCMC) method [27–29] is used to determine the position of liquid-vapor equilibrium. In the MCMC method, two simulation cells of fixed volume are used, one representing the pore (the same as in GCMC simulations) and the other used as a gauge cell to measure the chemical potential corresponding to given adsorbed amount. The MCMC method allows for the construction of the continuous canonical ensemble isotherm of a van der Waals type sigmoidal shape. The canonical ensemble isotherm connects the stable and metastable states by a trajectory of the states that are unstable in the open system, which are stabilized by suppressing density fluctuations by the finite size gauge cell. The equilibrium pressure is calculated by applying Maxwell's rule of equal areas. In addition, the energy barrier separating the equilibrium vapor-like and liquidlike states are estimated by the thermodynamic integration. The energy barrier indicates whether the adsorption-desorption hysteresis may be present in experiments. As shown in our previous work, ³⁶ the experimental hysteresis may be observed if the energy barrier in MC simulations exceeds the critical energy barrier of ~43 kT. At smaller barriers, the experimental isotherm is reversible. For details of the implementation of the MCMC method, see our previous work [40].

Saturation pressure CO_2 at 273.15 K in the MC simulations calculated as $P_0 = 34.94$ bar (slightly exceeding the experimental value of 34.85 bar) is used to normalize the simulated adsorption isotherms as functions of the relative pressure P/P_0 .

3. Results and discussion

3.1. Simulation results

Two kernels of reference equilibrium adsorption isotherms of CO_2 at 273.15 K were constructed using the model previously validated by adsorption on graphitic surface [40]. First "cylindrical" kernel is composed of the isotherms in cylindrical pores ranging from 0.385 to 10 nm. Second "slit-cylindrical" kernel combines the isotherms in slit-shaped micropores from 0.385 to 2 nm and in cylindrical mesopores from 2.1 to 10 nm. The kernel isotherms are shown on Fig. 1. Each kernel contains 87 isotherms, and each isotherm contains at least 100 simulation points at relative pressure from $p/p_0 = 10^{-9}$ up to saturation, $p/p_0 = 1$. The kernel isotherms are smoothened and interpolated to achieve the same 600-point pressure grid. The procedure of kernel construction from the array of the simulated data points is presented in Supplementary Information, section A.

Adsorption isotherms for pores larger than 5.5 nm start showing adsorption hysteresis tracing metastable states along the adsorption and desorption isotherms leading to the stepwise spontaneous capillary condensation and evaporation (cavitation), respectively. In Fig. 2, the 8 nm pore was chosen to showcase the hysteresis behavior. The adsorption and desorption branches obtained by GCMC simulations are shown by closed and open black circles connected by black lines. The van-der-Waals type continuous

sigmoidal isotherm generated by the MCMC method is shown by grey dots connected by the broken grey line. The equilibrium pressure (Peq) calculated from the Maxwell rule of equal areas is shown by the broken red line. Close and open green circles correspond to the smoothened adsorption and equilibrium isotherms that are used in the kernel of the generalized adsorption equation (1). A close inspection on the graph in Fig. 2 reveals a hysteresis loop formed by the GCMC isotherm of width $\sim 0.05 p/p_0$ between the adsorption and desorption branches. The energy barrier for the condensation transition at equilibrium was calculated to be ~14 kT for this particular pore size. This barrier is much smaller than the previously calculated critical energy barrier of ~43 kT, indicating that the condensation under experimental conditions happens at the same pressure as evaporation and the adsorption-desorption isotherm is reversible [40]. This is in line with the reversible behavior observed in the experiments using CO₂ adsorption at 273 K in the materials studied in this work, see Fig. 4c below.

The pore filling pressure is defined as the adsorption isotherm inflection point (most micropores), the capillary condensation pressure (mesopores <5.5 nm), or the vapor-liquid equilibrium pressure (mesopores >5.5 nm). Fig. 3 shows the pore size dependence of the filling pressures in the kernel isotherms in pores of slit-shaped and cylindrical geometries. The dependency of the filling pressures with pore sizes is qualitatively equivalent to what is observed for Ar and N $_2$ using QSDFT [26]. Noteworthy, the filling pressure for large mesopores (>6 nm) changes very gradually that, as shown below, decreases the resolution of the pore size determination.

3.2. Experimental adsorption data

The experimental adsorption data for N₂, Ar, and CO₂ adsorption on three CMK-3 carbon samples (CMK-3a, CMK-3b, CMK-3c) is shown in Fig. 4. As these samples are the inverse replicas of their ordered mesoporous silicas counterparts, their pore network structure is comprised of cylindrical rods connected by crossbars. The complex-shaped mesopore channels are conventionally modeled assuming simple cylindrical geometry that was proven practical for the pore size characterization by Ar and N2 adsorption, as the resulting PSDs agreed with the XRD data [43]. The microporosity is developed during the templating process. The more incomplete the transformation is, the more micropores are present on the final structure. The micropores can be described by either as slit-shaped or cylindrical pores, depending on the structural specifics of the material. While the Ar and N2 isotherms exhibit prominent capillary condensation hysteresis, the CO2 isotherms are reversible. The absence of the hysteresis is explained by the proximity of the experimental temperature (273 K) to the pore critical temperature, i.e. it is known that for a given mesopore size hysteresis disappears at the so-called hysteresis critical temperature which is below, but close to the pore critical temperature that caused high level of density fluctuations and small energy barriers that can be crossed during the time of equilibration.

3.3. Sample characterization by gas adsorption

The MC simulated kernels of CO₂ isotherms at 273 K (Fig. 1) are used to calculate the PSDs of the CMK-3 samples CMK-3a, CMK-3b, and CMK-3c. The results are displayed in Fig. 5, showcasing the differential and cumulative PSDs using the cylindrical kernel (left panel), and the hybrid slit-cylindrical kernel (right panel). The CO₂ PSDs are compared with the benchmark PSDs obtained from Ar and N₂ isotherms using the standard N₂ and Ar QSDFT kernels [43] and indeed good agreement can be observed, particularly in the mesopore region.

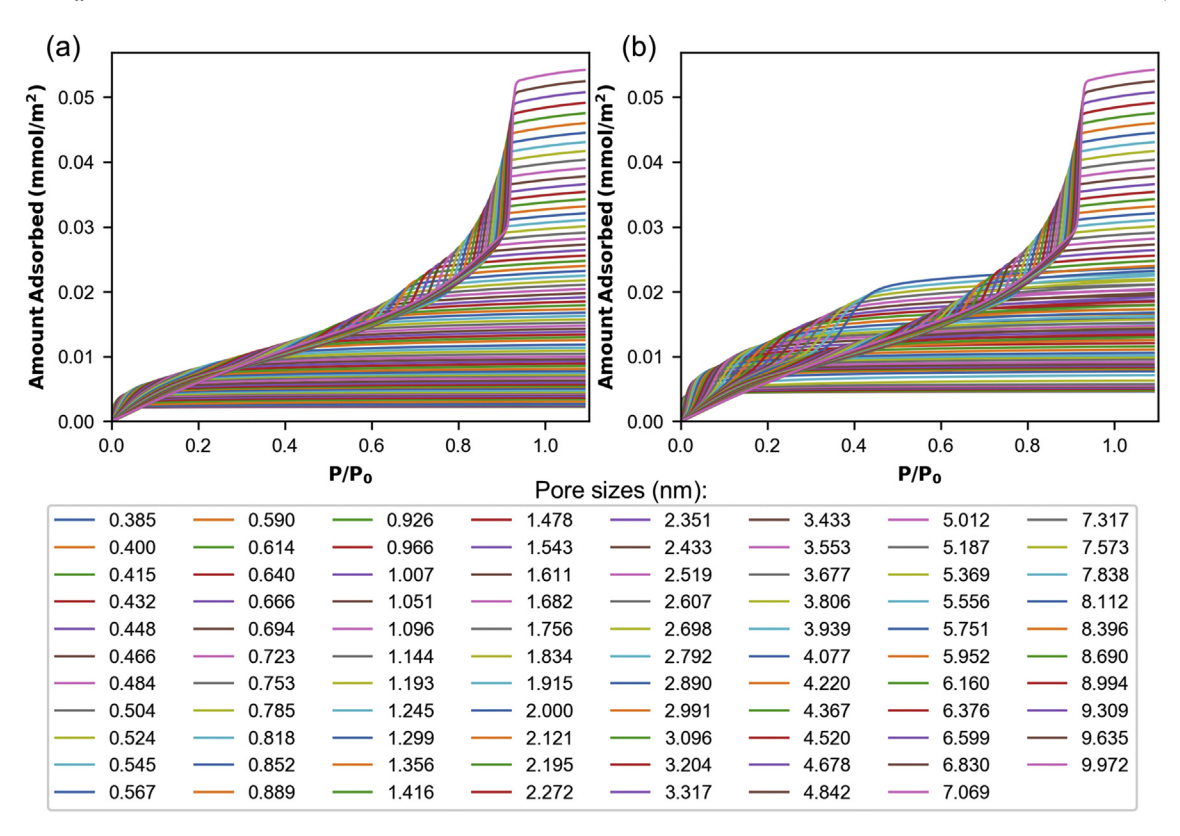


Fig. 1. The kernels of MC simulated equilibrium adsorption isotherms of CO_2 at 273 K in model carbon pores of 87 diameters (a) kernel of isotherms in cylindrical pores, and (b) combined kernel of isotherms in slit-shaped micropores (<2 nm) and cylindrical mesopores (>2 nm). (A colour version of this figure can be viewed online.)

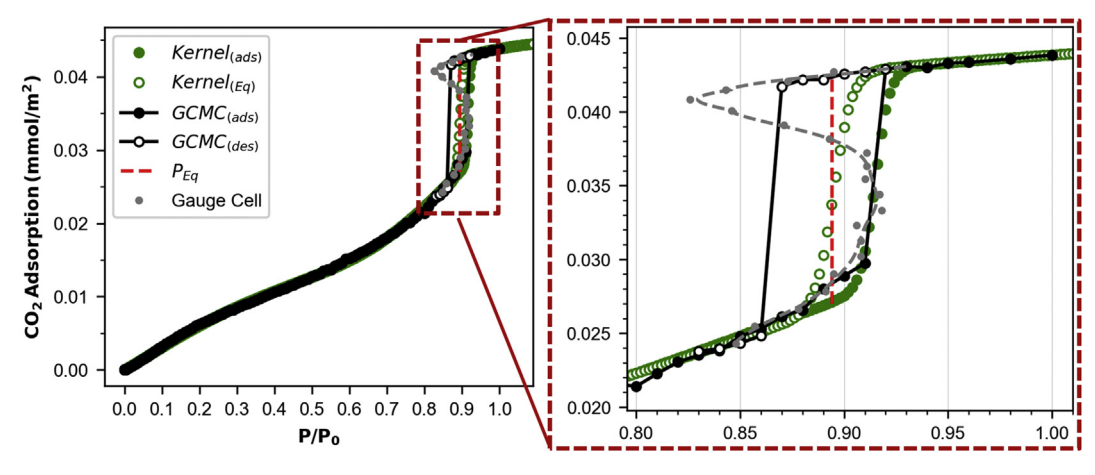


Fig. 2. Simulated adsorption isotherm of CO₂ in cylindrical carbon pore at 273 K highlighting the differences between equilibrium and adsorption branches. (A colour version of this figure can be viewed online.)

The micropore region is where the CO_2 shows its capacity to probe even smaller pores for CMK-3a and CMK-3b when compared against N_2 and Ar, although the overall micropore volume obtained from CO_2 data is very similar to the corresponding values obtained from N_2 and Ar. In Fig. 5 (right column), we show the PSDs using a combination of slit and cylindrical pore models for the three samples, where the micropores (0.385-2~nm) have slit shape and the mesopores (2-10~nm). In the mesopore region, the PSDs from Ar and N_2 are very similar, while the results from CO_2 at 273 K follow very closely, especially for CMK-3a and CMK-3b. In the micropore region, CO_2 is able to probe the smallest pores of CMK-3a and CMK-3b, compared to N_2 and Ar, although the overall

micropore volume obtained from the CO_2 isotherms is very similar to the corresponding values obtained from the N_2 and Ar isotherms. The PSDs from CO_2 show one complete main peak distribution below 2 nm for all three samples, with small peaks around 2 nm from the stitching of the two types of pore models into the same kernel. This is a better representation of the pore space in these samples when compared to Ar and N_2 . Additionally, all methods produce the same pore volume for all samples.

The existing methods for PSD calculations from low pressure (<1 atm) CO₂ isotherms are limited by the range of narrow pores (< ca. 1 nm), which are filled at relative pressure, p/p_0 , below ca. 3 \times 10⁻². In case of samples with larger micropores, and especially, for

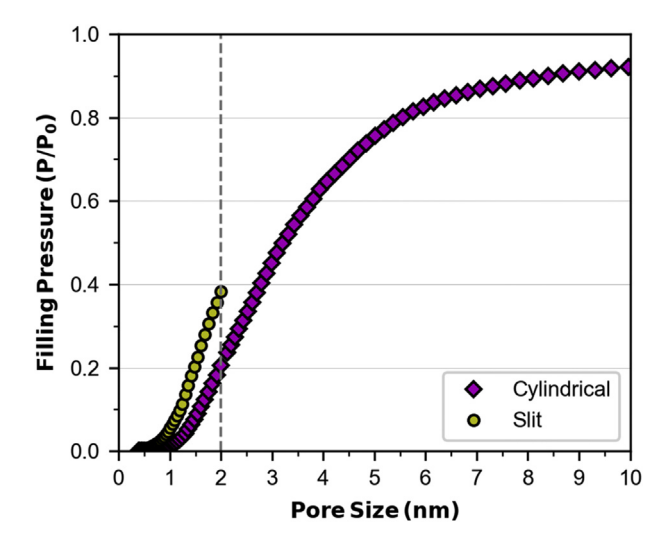


Fig. 3. Equilibrium filling pressures for CO_2 adsorption at 273.15 κ in carbon pores. (A colour version of this figure can be viewed online.)

samples with a wide range of pore sizes (as the micro-mesoporous CMK-3 carbons considered here), these methods produce unreliable PSDs in the region of supermicropores (>~1 nm). A characteristic example of comparison of the micropore size distributions for sample CMK-3c calculated with the high-pressure kernel (this work) and the low-pressure MC kernel from Ref. [22] is shown in Supplementary Information, section B.

An intrinsic problem for CO₂ pore size analysis at 273 K arises from the correlation between pore size and relative pressure for pore filling/condensation, as shown in Fig. 3. Due to the fact that CO₂ is at 273 K, relatively close to the critical temperature (e.g. T/ Tc = 0.9 compared to T/Tc = 0.61 for N_2 at 77 K, and T/Tc = 0.58 for Ar at 87 K), the relationship between pore filling pressure and pore size becomes quite unsensitive starting already at pores of diameter >6 nm as indicated in the substantial flattening of the curve. Hence, small variations in p/p_0 are correlated with large changes in the pore size. In fact, the established pore size dependence of the filling pressure in Fig. 3 suggests that pores in the order of 10 nm would fill at the pressures extremely close to the bulk saturation pressure, limiting the experimentally accessible pore size range for pore size analysis with CO2 at 273 K. Consequently, relatively small uncertainties in the effective experimental saturation pressure leads to appreciable shifts in the calculated pore size distribution, as discussed in section C of the Supplementary information. This factor affects the PSD calculated for the CMK-3 sample, Fig. 5c, where the predicted main mesopore peak is around 6.5 nm, slightly larger than the obtained by Ar and N₂ analysis. Furthermore, a reduction in experimental temperature is desirable in order to enlarge the practically accessible pore size range based on CO2 adsorption. Such work is in progress based on the fundamental study of the temperature behavior of CO₂ adsorption/condensation in mesoporous carbons [40].

4. Conclusions

We present a Monte Carlo simulated kernel of CO₂ adsorption isotherms at 273 K in the range of pressures up to the saturation pressure (34.85 bar), covering a wide range of micro- and mesopores (0.385–10 nm). This method enables, for the first time, a combined micro-mesopore analysis of nanoporous carbons solely with CO₂ adsorption at 273 K. Using CO₂ as a molecular probe allows to directly determine the distribution of pores accessible to

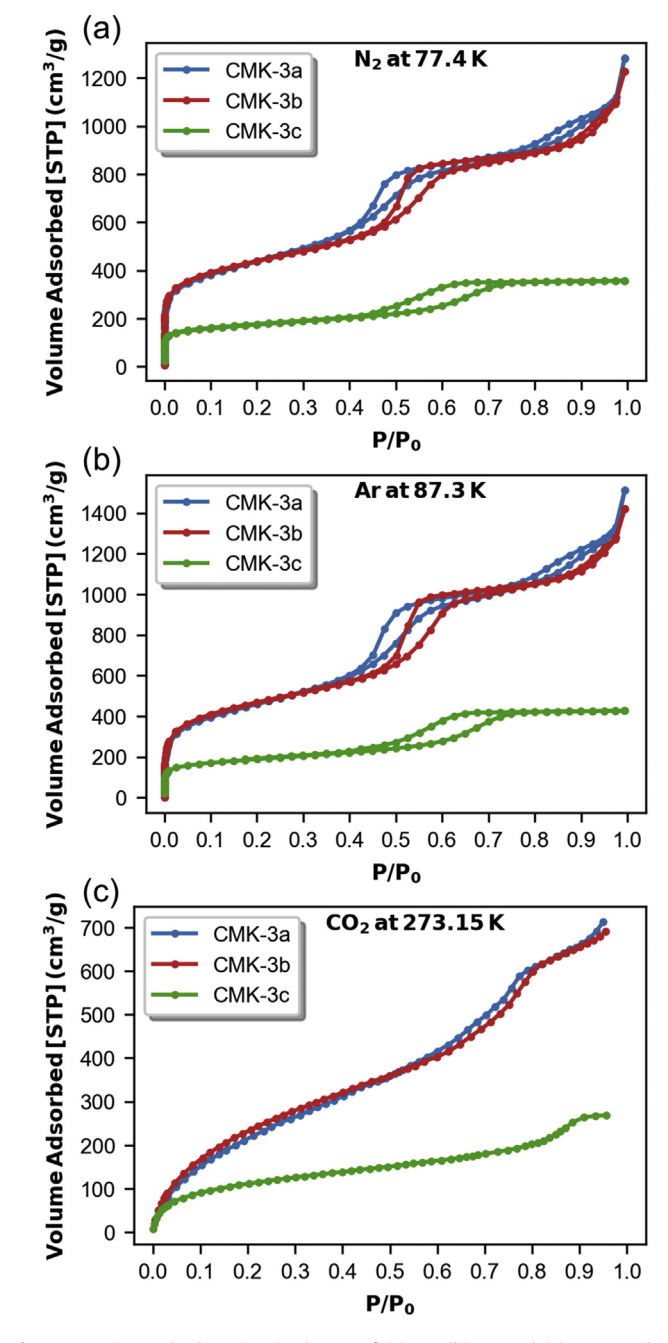


Fig. 4. Experimental adsorption isotherms of (a) N_2 , (b) Ar, and (c) CO_2 on three samples of CMK-3: CMK-3a, CMK-3b, and CMK-3c. (A colour version of this figure can be viewed online.)

 ${\rm CO_2}$ and their maximum capacity in the wide range of pressures that may inform the choice of adsorbents for ${\rm CO_2}$ capture and storage.

The key innovation here stems from the possibility of obtaining information about a wide range of micro and mesopores with one adsorption experiment. The method incorporates an atomistic model for CO_2 combined with an integrated potential to represent the fluid-solid interactions. In this manner, we can properly describe the adsorption behavior in both micro and mesopore regions, especially the capillary condensation and hysteresis behavior in larger mesopores. Our study also reveals intrinsic limitations for the application range of CO_2 adsorption at 273 K ($T/T_{c,bulk} = 0.9$) for a combined micro-mesopore system based on the predicted

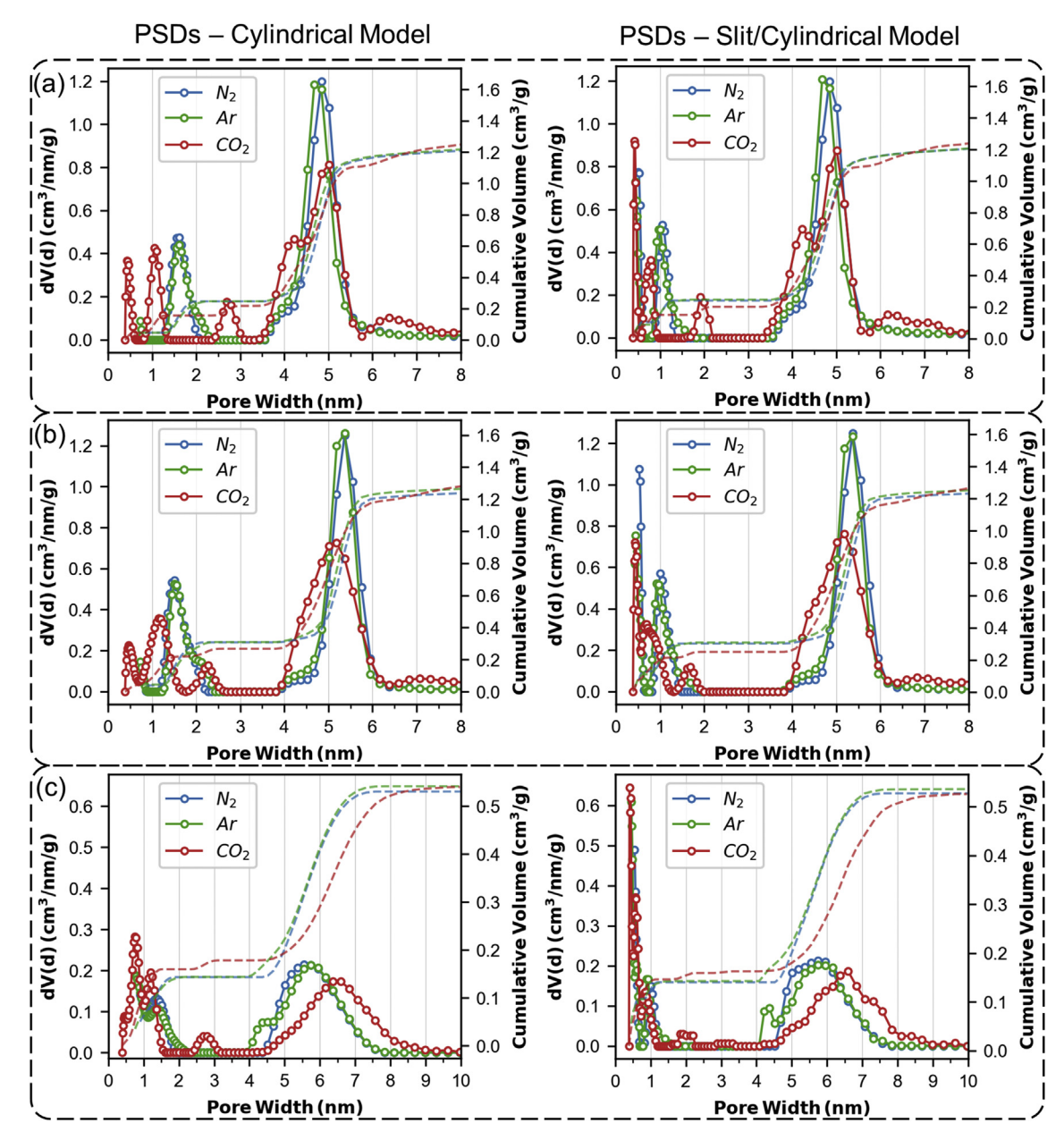


Fig. 5. Pore size distributions for (a) CMK-3a, (b) CMK-3b, and (c) CMK-3c samples using a cylindrical pore model kernel (left column), and slit pore model for micropores and cylindrical pore model for mesopores (right column). (A colour version of this figure can be viewed online.)

correlation between the pore size and the pore filling pressure. In fact, the relative pressure of pore filling for pores larger than 6 nm shifts quite close to the saturation pressure with large differences in the pore size corresponding to very small changes in the pore filling pressure. This intrinsic fact coupled with the resulting experimental challenges limits CO₂ pore size analysis at 273 K to the upper pore size of ca. 10 nm. Hence, lower experimental temperatures for CO₂ carbon pore size analysis are needed for enhancing the accessible upper mesopore size range. At the same time, the chosen temperature should still assure fast diffusion into ulramicropores.

CRediT authorship contribution statement

Silvio Dantas: Methodology, Validation, Formal analysis, Investigation, Writing - original draft. **Katie Cychosz Struckhoff:**

Investigation, Formal analysis, Data curation. **Matthias Thommes:** Methodology, Investigation, Formal analysis, Writing - review & editing. **Alexander V. Neimark:** Conceptualization, Methodology, Investigation, Writing - review & editing.

Declaration of competing interest

The authors declare that they have no known competing financial interests or personal relationships that could have appeared to influence the work reported in this paper.

Acknowledgement

This work is supported in part by the National Science Foundation (grant No 1834339 to AVN).

Appendix A. Supplementary data

Supplementary data to this article can be found online at https://doi.org/10.1016/j.carbon.2020.11.059.

References

- J. Garrido, A. Linares-Solano, J.M. Martin-Martinez, M. Molina-Sabio, F. Rodriguez-Reinoso, R. Torregrosa, Use of nitrogen vs. carbon dioxide in the characterization of activated carbons, Langmuir 3 (1) (1987) 76–81, https:// doi.org/10.1021/la00073a013.
- [2] F. Rodriguez-Reinoso, An overview of methods for the characterization of activated carbons, Pure Appl. Chem. 61 (11) (1989) 1859–1866, https:// doi.org/10.1351/pac198961111859.
- [3] R.V.R.A. Rios, J. Silvestre-Albero, A. Sepulveda-Escribano, M. Molina-Sabio, F. Rodriguez-Reinoso, Kinetic restrictions in the characterization of narrow microporosity in carbon materials, J. Phys. Chem. C 111 (10) (2007) 3803–3805, https://doi.org/10.1021/jp0701486.
- [4] M. Thommes, K.A. Cychosz, A.V. Neimark, Advanced physical adsorption characterization of nanoporous carbons, in: J.M.D. Tascon (Ed.), Novel Carbon Adsorbents, Elsevier, 2012, pp. 107–145, https://doi.org/10.1016/B978-0-08-097744-7.00004-1.
- [5] M. Thommes, K. Kaneko, A.V. Neimark, J.P. Olivier, F. Rodriguez-Reinoso, J. Rouquerol, et al., Physisorption of gases, with special reference to the evaluation of surface area and pore size distribution (IUPAC Technical Report), Pure Appl. Chem. 87 (9–10) (2015) 1051–1069, https://doi.org/10.1515/pac-2014-1117.
- [6] P.N.K. De Silva, P.G. Ranjith, S.K. Choi, A study of methodologies for CO2 storage capacity estimation of coal, Fuel 91 (1) (2012) 1–15, https://doi.org/ 10.1016/i.fuel.2011.07.010.
- [7] C. Stoquart, P. Servais, P.R. Berube, B. Barbeau, Hybrid Membrane Processes using activated carbon treatment for drinking water: a review, J. Membr. Sci. 411–412 (2012) 1–12, https://doi.org/10.1016/j.memsci.2012.04.012.
- [8] M.H. Sun, S.Z. Huang, L.H. Chen, Y. Li, X.Y. Yang, Z.Y. Yuan, et al., Applications of hierarchically structured porous materials from energy storage and conversion, catalysis, photocatalysis, adsorption, separation, and sensing to biomedicine, Chem. Soc. Rev. 45 (12) (2016) 3479–3563, https://doi.org/ 10.1039/c6cs00135a.
- [9] K. Zhu, J. Sun, H. Zhang, J. Liu, Y. Wang, Carbon as a hard template for nano material catalysts, J. Nat. Gas Chem. 21 (3) (2012) 215–232, https://doi.org/ 10.1016/s1003-9953(11)60357-5.
- [10] W. Fan, M.A. Snyder, S. Kumar, P.S. Lee, W.C. Yoo, A.V. McCormick, et al., Hierarchical nanofabrication of microporous crystals with ordered mesoporosity, Nat. Mater. 7 (12) (2008) 984–991, https://doi.org/10.1038/ pp. 12303
- [11] B. Fang, J.H. Kim, M.S. Kim, J.S. Yu, Hierarchical nanostructured carbons with meso-macroporosity: design, characterization, and applications, Acc. Chem. Res. 46 (7) (2013) 1397–1406, https://doi.org/10.1021/ar300253f.
- [12] S. Qiu, J.W. Zheng, G.T. Yang, J.T. Zheng, M.B. Wu, W.T. Wu, Synthesis and application of three-dimensionally ordered macroporous carbon with designed pore architecture, Prog. Chem. 26 (5) (2014) 772–783, https:// doi.org/10.7536/PC131104.
- [13] D. Zhao, J. Feng, Q. Huo, N. Melosh, G.H. Fredrickson, B.F. Chmelka, et al., Triblock copolymer syntheses of mesoporous silica with periodic 50 to 300 angstrom pores, Science 279 (5350) (1998) 548–552, https://doi.org/10.1126/ science.279.5350.548.
- [14] C.A. Fyfe, G.Y. Fu, Structure organization of silicate polyanions with surfactants: a new approach to the syntheses, structure transformations, and formation mechanisms of mesostructural materials, J. Am. Chem. Soc. 117 (38) (1995) 9709–9714, https://doi.org/10.1021/ja00143a014.
- [15] S. Jun, S.H. Joo, R. Ryoo, M. Kruk, M. Jaroniec, Synthesis of new, nanoporous carbon with hexagonally ordered mesostructure, J. Am. Chem. Soc. 122 (43) (2000) 10712–10713, https://doi.org/10.1021/ja002261e.
- [16] K.A. Cychosz, R. Guillet-Nicolas, J. Garcia-Martinez, M. Thommes, Recent advances in the textural characterization of hierarchically structured nanoporous materials, Chem. Soc. Rev. 46 (2) (2017) 389–414, https://doi.org/10.1039/c6cs00391e.
- [17] D. Cazorla-Amoros, J. Alcaniz-Monge, A. Linares-Solano, Characterization of activated carbon fibers by CO2Adsorption, Langmuir 12 (11) (1996) 2820–2824, https://doi.org/10.1021/la960022s.
- [18] F. Rouquerol, J. Rouquerol, K. Sing, Adsorption by Powders and Porous Solids: Principles, Methodology and Applications, Academic Press, London, 1999, https://doi.org/10.1016/B978-0-12-598920-6.X5000-3.
- [19] E.W. Lemmon, M.O. McLinden, D.G. Friend, Thermophysical Properties of Fluid Systems, NIST Chemistry WebBook, NIST Standard Reference Database Number 69, Eds. P.J. Linstrom and W.G. Mallard, National Institute of Standards and Tech, Gaithersburg MD, 20899, https://doi.org/10.18434/T4D303,

- (retrieved September 24, 2020).
- [20] J. Landers, G.Y. Gor, A.V. Neimark, Density functional theory methods for characterization of porous materials, Colloids Surf. A Physicochem. Eng. Asp. 437 (2013) 3–32, https://doi.org/10.1016/j.colsurfa.2013.01.007.
- [21] A. Vishnyakov, P.I. Ravikovitch, A.V. Neimark, Molecular level models for CO₂ sorption in nanopores, Langmuir 15 (25) (1999) 8736–8742, https://doi.org/10.1021/la990726c.
- [22] P.I. Ravikovitch, A. Vishnyakov, R. Russo, A.V. Neimark, Unified approach to pore size characterization of microporous carbonaceous materials from N₂, Ar, and CO₂ adsorption isotherms, Langmuir 16 (5) (2000) 2311–2320, https://doi.org/10.1021/la991011c.
- [23] J.P. Toso, R.H. Lopez, D.C.S. de Azevedo, C.L. Cavalcante, M.J. Prauchner, F. Rodriguez-Reinoso, et al., Evaluation of a mixed geometry model for the characterization of activated carbons, Adsorption 17 (3) (2011) 551–560, https://doi.org/10.1007/s10450-011-9324-8.
- [24] V. Yelpo, V. Cornette, J.P. Toso, R.H. Lopez, Characterization of nanostructured carbon CMK-3 by means of Monte Carlo simulations, Carbon 121 (2017) 106–113, https://doi.org/10.1016/j.carbon.2017.05.085.
- [25] P.I. Ravikovitch, A.V. Neimark, Density functional theory model of adsorption on amorphous and microporous silica materials, Langmuir 22 (26) (2006) 11171–11179, https://doi.org/10.1021/la0616146.
- [26] A.V. Neimark, Y. Lin, P.I. Ravikovitch, M. Thommes, Quenched solid density functional theory and pore size analysis of micro-mesoporous carbons, Carbon 47 (7) (2009) 1617–1628, https://doi.org/10.1016/j.carbon.2009.01.050.
- [27] A.V. Neimark, A. Vishnyakov, Gauge cell method for simulation studies of phase transitions in confined systems, Phys. Rev. 62 (4 Pt A) (2000) 4611–4622, https://doi.org/10.1103/physreve.62.4611.
- [28] A. Vishnyakov, A.V. Neimark, Studies of Liquid-Vapor equilibria, criticality, and spinodal transitions in nanopores by the gauge cell Monte Carlo simulation method, J. Phys. Chem. B 105 (29) (2001) 7009-7020, https://doi.org/ 10.1021/jp0039940.
- [29] A.V. Neimark, A. Vishnyakov, A simulation method for the calculation of chemical potentials in small, inhomogeneous, and dense systems, J. Chem. Phys. 122 (23) (2005) 234108, https://doi.org/10.1063/1.1931663.
- [30] S.H. Joo, R. Ryoo, M. Kruk, M. Jaroniec, Evidence for general nature of pore interconnectivity in 2-dimensional hexagonal mesoporous silicas prepared using block copolymer templates, J. Phys. Chem. B 106 (18) (2002) 4640–4646, https://doi.org/10.1021/jp013583n.
- 4640–4646, https://doi.org/10.1021/jp013583n.
 P.I. Ravikovitch, D. Wei, W.T. Chueh, G.L. Haller, A.V. Neimark, Evaluation of pore structure parameters of MCM-41 catalysts supports and catalysts by means of nitrogen and argon adsorption, J. Phys. Chem. B 101 (19) (1997) 3671–3679, https://doi.org/10.1021/jp9625321.
- [32] A.N. Tikhonov, On the stability of inverse problems, Dokl. Akad. Nauk SSSR 39 (1943) 176–179.
- [33] C.L. Lawson, R.J. Hanson, Solving Least Squares Problems, SIAM, Philadelphia, Pa, 1995, https://doi.org/10.1137/1.9781611971217.
- [34] H. Huwe, M. Froba, Iron(III) oxide nanoparticles within the pore system of mesoporous carbon CMK-1: intra-pore synthesis and characterization, Microporous Mesoporous Mater. 60 (1–3) (2003) 151–158, https://doi.org/10.1016/3187-1811(03)00336-6.
- [35] M. Thommes, J. Morell, K.A. Cychosz, M. Froba, Combining nitrogen, argon, and water adsorption for advanced characterization of ordered mesoporous carbons (CMKs) and periodic mesoporous organosilicas (PMOs), Langmuir 29 (48) (2013) 14893–14902, https://doi.org/10.1021/la402832b.
- [36] R. Ryoo, S.H. Joo, S. Jun, Synthesis of highly ordered carbon molecular sieves via template-mediated structural transformation, J. Phys. Chem. B 103 (37) (1999) 7743-7746, https://doi.org/10.1021/jp991673a.
- [37] G.J. Tjatjopoulos, D.L. Feke, J.A. Mann, Molecule-micropore interaction potentials, J. Phys. Chem. 92 (13) (1988) 4006–4007, https://doi.org/10.1021/i100324a063
- [38] W.A. Steele, The physical interaction of gases with crystalline solids, Surf. Sci. 36 (1) (1973) 317–352, https://doi.org/10.1016/0039-6028(73)90264-1.
- [39] J.J. Potoff, J.I. Siepmann, Vapor—liquid equilibria of mixtures containing alkanes, carbon dioxide, and nitrogen, AlChE J 47 (7) (2001) 1676–1682, https://doi.org/10.1002/aic.690470719.
- [40] S. Dantas, K.C. Struckhoff, M. Thommes, A.V. Neimark, Phase behavior and capillary condensation hysteresis of carbon dioxide in mesopores, Langmuir 35 (35) (2019) 11291–11298, https://doi.org/10.1021/acs.langmuir.9b01748.
- [41] E.J. Bottani, V. Bakaev, W. Steele, A simulation/experimental study of the thermodynamic properties of carbon dioxide on graphite, Chem. Eng. Sci. 49 (17) (1994) 2931–2939, https://doi.org/10.1016/0009-2509(94)e0111-3.
- [42] M.G. Martin, MCCCS Towhee: a tool for Monte Carlo molecular simulation, Mol. Simulat. 39 (14–15) (2013) 1212–1222, https://doi.org/10.1080/ 08927022.2013.828208.
- [43] G.Y. Gor, M. Thommes, K.A. Cychosz, A.V. Neimark, Quenched solid density functional theory method for characterization of mesoporous carbons by nitrogen adsorption, Carbon 50 (4) (2012) 1583–1590, https://doi.org/10.1016/ j.carbon.2011.11.037.